

A CATALOG OF BACKGROUND STARS REDDENED BY DUST IN THE TAURUS DARK CLOUDS

S. S. Shenoy^{1,2}, D. C. B. Whittet¹, J. A. Ives¹, and D. M. Watson³

ABSTRACT

Normal field stars located behind dense clouds are a valuable resource in interstellar astrophysics, as they provide continua in which to study phenomena such as gas-phase and solid-state absorption features, interstellar extinction and polarization. This paper reports the results of a search for highly reddened stars behind the Taurus Dark Cloud complex. We use the Two Micron All Sky Survey (2MASS) Point Source Catalog to survey a ~ 50 deg² area of the cloud to a limiting magnitude of $K_s = 10.0$. Photometry in the 1.2–2.2 μm passbands from 2MASS is combined with photometry at longer infrared wavelengths (3.6–12 μm) from the *Spitzer Space Telescope* and the *Infrared Astronomical Satellite* to provide effective discrimination between reddened field stars and young stellar objects (YSOs) embedded in the cloud. Our final catalog contains 248 confirmed or probable background field stars, together with estimates of their total visual extinctions, which span the range $2 < A_V < 29$ mag. We also identify the 2MASS source J04292083+2742074 (IRAS 04262+2735) as a previously unrecognized candidate YSO, based on the presence of infrared emission greatly in excess of that predicted for a normal reddened photosphere at wavelengths $> 5 \mu\text{m}$.

Subject headings: Infrared: stars — dust, extinction — ISM: clouds — ISM: individual (Taurus Dark Cloud)

¹Department of Physics, Applied Physics & Astronomy, Rensselaer Polytechnic Institute, 110 Eighth Street, Troy, NY 12180.

²Present address: Spitzer Science Center, Mail Code 220–6, California Institute of Technology, Pasadena, CA 91125. Email: sshenoy@ipac.caltech.edu.

³Department of Computer Science, Rensselaer Polytechnic Institute, 110 Eighth Street, Troy, NY 12180.

1. Introduction

Observations of many interstellar phenomena rely on the presence of background field stars, i.e. stars lying beyond the region of interest that provide sources of continuum radiation. Examples include absorption-line spectroscopy of ionic, atomic and molecular gas, spectroscopy of solid-state absorption features in dust grains, and the continuum effects of interstellar extinction and polarization introduced by dust, at wavelengths extending from the far ultraviolet to the mid-infrared. Observations at ultraviolet and visible wavelengths are generally limited to lines of sight with low to moderate extinction and therefore sample mostly diffuse phases of the interstellar medium (ISM). Observations in the near to mid-infrared allow studies of these absorptive phenomena to be extended to dense molecular clouds, where they provide information complementary to that obtained at much longer wavelengths where cool dust and gas can be observed in emission in their own right.

Observing absorption features in discrete lines of sight toward background stars places an obvious limitation on spatial resolution. Consider, for example, the distribution of molecular gas in cold, dense clouds, and the depletion of molecules onto the surfaces of dust grains to form icy mantles. Radio astronomers can readily map the distribution of molecular gas by observing its intensity in a chosen spectral emission line (most commonly of CO) at a spatial resolution limited only by the beam of the telescope (see Mizuno et al. 1995 for an example relevant to the current work). However, to map the corresponding distribution of molecular solids one must study an infrared absorption feature, such as the $3.0\ \mu\text{m}$ feature of solid H_2O , against a continuum provided by a background star. The first attempt to map the ice distribution by this method, that of Murakawa et al. (2000), was limited to detections of the $3.0\ \mu\text{m}$ feature in some 25 lines of sight in the Heiles Cloud 2 region of Taurus. At mid-infrared wavelengths, it is possible to study interstellar absorptions against extended background emission, as described by Sonnentrucker et al. (2008) for the $15\ \mu\text{m}$ feature of CO_2 ; but this opportunity arises only in a limited number of cases, where cold material is located fortuitously in front of warmer material heated to appropriate temperatures by nearby luminous stars. In regions of low-mass star formation a point-like stellar continuum source is generally the only option. Interstellar absorption features are observed routinely in the spectra of young stellar objects (YSOs) embedded in the clouds (e.g. Boogert et al. 2004), but in these lines of sight ambiguity often exists between interstellar matter and material local to the source that may be modified by its presence. Only background stars provide the means of studying absorptions arising in quiescent regions of the dense ISM, remote from sources of radiation.

A primary motivation for infrared surveys of dark clouds is to conduct a census of star formation, in which YSOs are carefully distinguished from field stars. The Taurus dark-

cloud complex is a key region in studies of low-mass star formation (e.g. Luhman et al. 2006; Güdel et al. 2007; Padgett et al. 2007), and also a valuable laboratory for studying interstellar molecules and dust (e.g. Pratap et al. 1997; Dickens et al. 2001; Whittet et al. 2001). It is nearby (~ 140 pc; Kenyon et al. 1994; Loinard et al. 2005) and situated at moderate Galactic latitude ($b \sim 15^\circ$), circumstances that aid both types of study: there is relatively little risk of confusion between stellar associations at different distances along the line of sight, compared with a region in the Galactic disk, and almost all of the interstellar extinction and absorption in the direction of the cloud arises in the cloud itself. The first infrared survey of the Taurus region to include a significant number of reddened background stars was that of Elias (1978), who identified about a dozen such objects that have since been observed intensively for interstellar absorption features (e.g. Whittet et al. 2007 and references therein).

In recent years, the task of identifying reddened field stars has been greatly facilitated by the availability of data from the *Two-Micron All-Sky Survey* (2MASS; Skrutskie et al. 2006) and from surveys at longer infrared wavelengths made with the *Spitzer Space Telescope* (e.g. Luhman et al. 2006). The goal of this paper is to use these resources to construct a much larger catalog of field stars reddened by dust in the Taurus dark-cloud complex than has previously been available.

2. Photometric data and associations

2.1. 2MASS

The survey area selected for this work, shown in Fig. 1, is based on the ^{13}CO (J=1–0) map of the Taurus cloud complex reported by Mizuno et al. (1995, their Fig. 3). Near-infrared photometric data in the $1.25\ \mu\text{m}$ (J), $1.65\ \mu\text{m}$ (H) and $2.17\ \mu\text{m}$ (K_s) passbands were compiled for stars within this survey area from the 2MASS survey¹. A limiting magnitude of $K_s = 10.0$ was adopted: this constraint ensures that only stars with highest-quality photometry are selected, and has the additional benefit of excluding background red dwarfs, thus avoiding a possible source of ambiguity in the intrinsic colors (see §4). Further quality control was provided by the various flags included in the 2MASS catalog. Only observations with read flag (`rd_flg`) values of 1, 2 or 3 were selected as being high quality detections with reliable astrometry and photometry. Other flags that deal specifically with the quality of the

¹The data were collected using the Gator web interface of the Infrared Science Archive operated by the Infrared Processing and Analysis Center (<http://irsa.ipac.caltech.edu/applications/Gator/>).

data are the photometric quality flag (`ph_qual`) and the contamination and confusion flag (`cc_flg`). We selected only data with a `ph_qual` value of “A” in each passband, signifying the best quality photometric data one can obtain with 2MASS. The `cc_flg` indicates whether the photometry and/or positional measurement of a source may be contaminated or biased due to the proximity to an image artifact or a nearby source of equal or greater brightness: we chose only objects with `cc_flg` = 0, indicating sources unaffected by known artifacts or confusion. Photometric errors in the resulting data are ± 0.03 mag or less in each passband.

The following color constraints were used to discriminate against unreddened stars and stars with anomalous colors in the 2MASS database:

$$(J - H) > 1.75 (H - K_s) - 0.04 \quad (1)$$

$$(J - H) < 1.75 (H - K_s) + 0.56 \quad (2)$$

$$H - K_s > 0.4. \quad (3)$$

The multiplicative constant 1.75 in eqs. 1 and 2 is based on the observed reddening law (see §3): these equations define the range of colors over which normal stars may be dereddened onto intrinsic color lines (Itoh et al. 1996), as illustrated in Fig. 2a. Discrimination against normal stars with little or no reddening is provided by Eq. 3, which effectively excludes those with visual extinctions $A_V < 3$ mag. This extinction limit corresponds approximately to the threshold extinction for detection of ices in the region (Whittet et al. 2001 and references therein).

Application of the above criteria resulted in selection of 293 sources. Stellar associations were sought in the SIMBAD database, and it was found that the sample included a substantial number of sources associated with previously known YSOs. As an additional check on the status of each target, our list was collated with comprehensive catalogs of YSOs in the Taurus region recently compiled from infrared and X-ray observations (Luhman et al. 2006; Güdel et al. 2007; Scelsi et al. 2007). A total of 40 known or probable YSOs and 4 variable stars of other types were excluded, reducing the sample to 249 sources. This final catalog is presented in Table 1, and the distribution of the sources on the sky is shown in Fig. 1. 2MASS identifications and photometry are listed in Table 1, together with IRAS associations, stellar associations and spectral types, as available from the literature, and additional infrared data described below.

2.2. IRAC

Images from the Infrared Array Camera (IRAC; Fazio et al. 2004) on board the *Spitzer Space Telescope* provide photometry in four passbands centered at 3.6, 4.5, 5.8 and 8.0 μm .

The star-formation survey reported by Luhman et al. (2006) is based on a photometric catalog containing some 450,000 sources in the Taurus region (the Taurus IRAC Point Source Archive), of which photometry for only ~ 160 confirmed YSOs has been published to date. The IRAC data were processed by the Wisconsin IRAC Pipeline developed for the GLIMPSE Galactic Plane Survey and the SAGE Large Magellanic Cloud Survey (see Luhman et al. 2006 for further details). The entire catalog was kindly made available to us by Barbara Whitney and Marilyn Meade, and is used here in combination with the 2MASS data to provide an additional constraint on the nature of our sample of candidate field stars (§3).

The IRAC Point Source Archive was supplied in ascii format and a custom web-based interface was constructed to facilitate access. Collation with our field star catalog yielded associations for 186 out of 249 objects: the area of sky covered by the IRAC observations (Fig. 1 in Luhman et al. 2006) is somewhat smaller than our survey area, thus some of our 2MASS candidates lack IRAC coverage. All available photometry is included in Table 1. A few of the brightest sources are saturated at 3.6 and 4.5 μm . Photometric errors are typically ± 0.05 mag or less in each passband.

3. Color-color diagrams

The $J - H$ vs. $H - K$ color-color diagram provides useful but imperfect discrimination between dust-embedded stars and stars with normal photospheres subject to reddening (see Itoh et al. 1996 and Gutermuth et al. 2004 for discussion and examples). $J - H$ is most sensitive to the photospheric temperature of the star, whereas $H - K$ is also sensitive to emission from a circumstellar shell or disk — provided the circumstellar material is sufficiently warm. A more stringent discriminant that recognizes the presence of cooler circumstellar matter is possible in cases where additional photometry at longer wavelengths is available: we follow Gutermuth et al. (2004) in adopting the $J - H$, $H - [4.5]$ diagram as a valuable complement to $J - H$, $H - K$. Both diagrams are plotted for our candidate field stars in Fig. 2. As a control sample, we plot confirmed Taurus YSOs on the same axes in Fig. 3, using data from Luhman et al. (2006). Photometric errors are typically comparable with or smaller than the size of the plotting symbol in all figures.

Diagonal lines in Figs. 2 and 3 are parallel to the expected displacement caused by interstellar reddening, and delimit the approximate area occupied by normal stars: stars in this zone may be dereddened onto intrinsic color lines. In the case of $J - H$, $H - K_s$, these lines (eqs. 1 and 2) have slope set to the reddening ratio $E_{J-H}/E_{H-K} = 1.75$ determined from observations of Taurus field stars (Whittet et al. 2007); the corresponding lines in $J - H$, $H - [4.5]$ assume the standard average interstellar extinction law (Whittet 2003) to

transform from $H - K_s$ to $H - [4.5]$. Intrinsic $J - H$ and $H - K_s$ colors are from Bessell & Brett (1988) with transformations from Carpenter (2001). Intrinsic $H - [4.5]$ colors are based on an interpolation between ground-based $H - L$ and $H - M$, colors and should be treated as no more than a rough guide to the loci of normal unreddened stars.

All of our candidate field stars fall within the “normal reddened photospheres” zone of the $J - H$, $H - K_s$ diagram (Fig. 2a) by definition, as this was included in the selection criteria (§2.1). Fig. 2b shows that all with IRAC data available also lie within the corresponding zone of the $J - H$, $H - [4.5]$ plot. This is in contrast to the distribution of YSOs (Fig. 3), many of which show a displacement toward the right, especially in $H - [4.5]$, characteristic of circumstellar excess emission affecting the longer-wavelength color index. We consider the distribution of our field-star candidates in Fig. 2b to be strong evidence that the large majority are, indeed, normal reddened field stars. Perusal of the data in Table 1 indicates that this conclusion is independent of our choice of [4.5] as the representative IRAC passband: for example, the [4.5] and [8.0] values generally agree to within ~ 0.2 mag, indicating no gross differences between $H - [4.5]$ and $H - [8.0]$.²

As a further test, we plot in Fig. 4 the $J - H$ vs. $H - [12]$ color-color diagram for 26 stars that have $12\ \mu\text{m}$ data available (see column 11 of Table 1 and associated footnotes). Photometric values were calculated from $12\ \mu\text{m}$ fluxes taken from the IRAS Point Source Catalog, as available (19 sources), using the method described in the IRAS Explanatory Supplement (1988). Fluxes at $12\ \mu\text{m}$ for seven additional stars were estimated from published spectra obtained with the Infrared Spectrometer (IRS) of the Spitzer Space Telescope (Whittet et al. 2007). YSOs catalogued by Luhman et al. (2006) that have IRAS associations are also included in Fig. 4 for comparison. The zones occupied by YSOs and by reddened field stars are particularly well separated in this diagram, confirming the field-star status of all but one of the 26 candidates in the subset. A clear anomaly is identified in the case of J04292083+2742074 (IRAS 04262+2735), however: it plots with the field stars in Fig. 2 and with the YSOs in Fig. 4. Further discussion of this object is deferred to §5.

The level of certainty with which field-star status is assigned to each object in Table 1 naturally varies according to the information available. A total of 188 stars have photometry in IRAC and/or $12\ \mu\text{m}$ passbands consistent with an absence of circumstellar dust. Considering infrared data alone, this set might be confused with evolved (class III) YSOs that have completed dispersal of their dusty envelopes; however, such stars are typically strong X-ray sources and these have been excluded from our catalog (§2). Least securely characterized are 56 stars that lack spectral classifications and have photometry only in the 2MASS passbands.

²J04292083+2742074 is the only major exception (see §5).

4. Extinction

The visual extinction (A_V) was estimated for each star in Table 1 from 2MASS photometry. A_V is related to the infrared color excess E_{J-K} by the relation

$$A_V = rE_{J-K} \quad (4)$$

where r is a factor that depends on the form of the extinction curve over the relevant wavelengths: a mean value $r = 5.3 \pm 0.3$ was determined by Whittet et al. (2001) for the Taurus cloud (for comparison, $r \approx 6.0$ in the diffuse ISM). For stars with known spectral classifications, E_{J-K} is determined routinely from observed and intrinsic colors to yield A_V . For stars lacking spectral classifications, $E_{J-K} = E_{J-H} + E_{H-K}$ is estimated from the observed locus in the $J - H$ vs. $H - K_s$ diagram (Fig. 2a) by extrapolation along the appropriate reddening vector onto intrinsic color lines. This generally provides unambiguous results, notwithstanding the separation of giant and dwarf intrinsic colors at late spectral types (Fig. 2a). Background stars bright enough to be included in our sample are expected to be predominantly either late-type (K, M) giants, which deredden onto the upper branch, or main-sequence stars earlier than K0; red dwarfs distant enough to be background to the cloud are predicted to be too dim at $2.2 \mu\text{m}$ to be selected³. Note that our method for evaluating A_V improves upon a “one fits all” intrinsic $J - K$ color adopted for background stars lacking spectral classifications in some previous literature (Tamura et al. 1987; Goodman et al. 1992). Several Taurus YSOs also have near infrared colors consistent with normal reddened photospheres (compare Figs. 2a and 3a): extinction estimates have been obtained for the 10 most reddened (those with $J - H > 2.5$), and results are listed in Table 2. Our A_V estimates for both field stars and YSOs are thought to be accurate to ± 0.5 mag or better.

A histogram of A_V values from Table 1 is plotted in Fig. 5. The sample of 249 stars is divided into one-magnitude bins (black columns). Also shown is the effect of adding 81 optically-selected reddened stars ($A_V > 0.5$) in Taurus from the extinction studies of Straizys & Meistas (1980) and Whittet et al. (2001), which cover a similar area of sky. The minimum occurring in the $A_V = 2-3$ mag bin is probably not real but a result of incomplete sampling: our color criteria for infrared-selected sources (§2) introduced a sharp cutoff for $A_V < 3$, and the optically-selected sample is expected to become increasingly incomplete for $A_V > 2$. Overall, the distribution shows a broad peak centered near $A_V = 3.5$, with a tail extending to $A_V \sim 10$, and sporadic higher values (19 field stars with $A_V > 10$).

³Dwarfs with extinction $A_V = 3$ mag and spectral types K5, M0 and M5 are predicted to have $K_s = 10.5$, 11.1 and 12.2 mag, respectively, at the distance of the cloud (140 pc), and are thus excluded by our $K_s = 10$ mag limit (§2).

The distribution on the sky of stars from Tables 1 and 2 is shown in Fig. 1, with extinction distinguished by plotting symbol in three groups: low ($2 < A_V < 5$), intermediate ($5 < A_V < 10$) and high ($A_V > 10$). As expected, lines of sight with high extinction generally cluster toward known condensations such as L1495, B18 and TMC-1. Lines of sight with low and intermediate extinction lie predominantly toward the outer boundaries of condensations, but some are more widely distributed. See Cambr esy (1999) and Padoan et al. (2002) for more detailed maps of extinction in the Taurus region based on optical star counts and statistical analysis of 2MASS data, respectively.

5. J04292083+2742074: A candidate YSO

The 2MASS source J04292083+2742074 is identified as a possible YSO from its anomalous position in the $J - H$ vs. $H - [12]$ diagram (Fig. 4), based on an association with IRAS point source 04262+2735. Perusal of the 2MASS database shows no other $2.2\ \mu\text{m}$ source within the error ellipse of the IRAS position of sufficient brightness to cause confusion, thus the association appears to be secure. To elucidate the nature of this object, its spectral energy distribution (SED) was constructed from all available photometry (2MASS, IRAC, IRAS) and plotted in Fig. 6. The SED of the prototypical reddened field star Elias 16 is also shown for comparison. A fit to each SED was calculated assuming model atmospheres from Kurucz (1992) with extinction from the Cardelli, Clayton & Mathis (1989) R_V -dependent empirical law ($R_V = A_V/E_{B-V}$ is the ratio of total to selective visual extinction). For Elias 16, we assume Kurucz model t4500g20p00 (appropriate to a K giant with $T_{\text{eff}} = 4500$ K) reddened to $A_V = 24$ mag with the $R_V = 4.0$ extinction law. For IRAS 04262+2735, the same effective temperature was assumed and SEDs were calculated for both giant and dwarf spectra (Kurucz models t4500g20p00 and t4500g50p00, respectively). In practice it was found that the two models gave closely similar results: only that based on the dwarf intrinsic spectrum is shown in Fig. 6, reddened to $A_V = 5$ mag with the $R_V = 4.0$ extinction law.

Our calculated spectrum for Elias 16 provides a reasonable match to the observed SED over the entire $1\text{--}30\ \mu\text{m}$ spectral range, allowing for the presence of $8\text{--}12\ \mu\text{m}$ silicate absorption (Bowey et al. 1998) not accounted for in the model. In contrast, the observed SED for IRAS 04262+2735 diverges systematically from the model for wavelengths $\lambda > 5\ \mu\text{m}$, indicating the presence of strong infrared excess relative to the expected flux from the reddened photosphere in the Rayleigh-Jeans limit. The spectral form of the excess is broadly consistent with emission from dust at temperature $T_{\text{dust}} \approx 350$ K, as illustrated in Fig. 6. The most probable explanation is that IRAS 04262+2735 is, indeed, a previously unrecognized YSO with a warm circumstellar envelope.

6. Conclusions

The main product of this work is the catalog presented in Table 1, which includes 248 confirmed or probable background field stars (and one probable new YSO). This catalog should prove to be a valuable resource for future observing programs. For example, virtually all the included sources are expected to show $3\ \mu\text{m}$ H₂O-ice absorption, based on the previously-known $A_V > 3$ threshold in the correlation of ice optical depth with extinction (Whittet et al. 1988, 2001). The distribution of ice may thus be mapped in more detail than was possible in the previous study of Murakawa et al. (2000). The $3\ \mu\text{m}$ feature also has potential for mapping magnetic fields within the clouds, by virtue of excess polarization observed at this wavelength when ice-mantled grains are aligned (Hough et al. 1988). This method is potentially more reliable than studies utilizing continuum polarization, as the ice feature is an unambiguous tracer of dense material in the line of sight (Whittet et al. 2008).

This research has made use of the NASA/IPAC Infrared Science Archive, which is operated by the Jet Propulsion Laboratory, California Institute of Technology, under contract with the National Aeronautics and Space Administration (NASA). The Two Micron All Sky Survey is a joint project of the University of Massachusetts and the Infrared Processing and Analysis Center, funded by NASA and the National Science Foundation. The Taurus IRAC Point Source Archive utilizes IRAC data processed from the Taurus Spitzer Legacy Survey (PID 3584, PI Deborah Padgett). We are grateful to Barbara Whitney and Marilyn Meade for making the unpublished IRAC data available to us. Extensive use was also made of the SIMBAD database, operated at CDS, Strasbourg, France. Financial support for this research was provided by NASA (grant NAG5-12750 and JPL/Caltech Support Agreement no. 1264149).

REFERENCES

- Bessell, M.S. & Brett, J.M. 1988, *PASP*, 100, 1134
- Boogert, A.C.A., et al. 2004, *ApJS*, 154, 359
- Bowey, J.E., Adamson, A.J., & Whittet, D.C.B. 1998, *MNRAS*, 298, 131
- Cambrésy, L. 1999, *A&A*, 345, 965
- Cardelli, J.A., Clayton G.C., & Mathis J.S. 1989, *ApJ*, 345, 245
- Carpenter, J.M. 2001, *AJ*, 121, 2851
- Dickens, J.E., Langer, W.D., & Velusamy, T. 2001, *ApJ*, 558, 693
- Elias, J.H. 1978, *ApJ*, 224, 857
- Fazio, G.G., et al. 2004, *ApJS*, 154, 10
- Gomez, M., Kenyon, S.J., & Hartmann, L. 1994, *AJ*, 107, 1850
- Goodman, A.A., Jones, T.J., Lada, E.A., & Myers P.C. 1992, *ApJ*, 399, 108
- Güdel, M., et al. 2007, *A&A*, 468, 353
- Gutermuth, R.A., et al. 2004, *ApJS*, 154, 374
- Hough, J.H., et al. 1988, *MNRAS*, 230, 107
- IRAS Explanatory Supplement 1988, NASA Publication RP–1190, ed. C.A. Beichman et al. (NASA, Washington DC)
- Itoh, Y., Tamura, M., & Gatley, I. 1996, *ApJ*, 465, L129
- Jones, B.F., & Herbig, G.H. 1979, *AJ*, 84, 1872
- Kenyon, S.J., Dobrzycka, D., & Hartmann, L. 1994, *AJ*, 108, 1872
- Kurucz, R.L. 1992, in *IAU Symp. 149, The Stellar Populations of Galaxies*, eds. B. Barbuy & A. Renzini (Dordrecht: Kluwer), 225
- Loinard, L., Mioduszewski, A.J., Rodriguez, L.F., González, R.A., Rodriguez, M.I., & Torres, R.M. 2005, *ApJ*, 619, L179

- Luhman, K.L., Whitney, B.A., Meade, M.R., Babler, B.L., Indebetouw, R., Bracker, S., & Churchwell, E.B. 2006, *ApJ*, 647, 1180
- Mizuno, A., Onishi, T., Nagahama, T., Ogawa, H., & Fukui, Y. 1995 *ApJ*, 445, L161
- Murakawa, K., Tamura, M., & Nagata, T. 2000, *ApJS*, 128, 603
- Padgett, D., et al. 2007, *AAS Abstract*, 211, 29.04
- Padoan, P., Cambr esy, L., & Langer, W. 2002, *ApJ*, 580, L57
- Pratap, P., Dickens, J.E., Snell, R.L., Miralles, M.P., Bergin, E.A., Irvine, W.M., & Schloerb, F.P. 1997, *ApJ* 486, 862
- Scelsi, L., Maggio, A., Micela, G., Briggs, K., & G udel, M. 2007, *A&A*, 473, 589
- Shenoy, S.S. 2003, Ph.D. thesis, Rensselaer Polytechnic Institute
- Skrutskie, M.F., et al. 2006, *AJ*, 131, 1163
- Sonnentrucker, P., et al. 2008, *ApJ*, in press
- Straizys, V., & Meistas, E. 1980, *Acta. Astron.*, 30, 541
- Strom, K.M., & Strom, S.E. 1994, *ApJ*, 424, 237
- Tamura, M., Nagata, T., Sato, S., & Tanaka, M. 1987, *MNRAS*, 224, 413
- Whittet, D.C.B., 2003, *Dust in the Galactic Environment* (Institute of Physics Publishing, Bristol, 2nd edn.)
- Whittet, D.C.B., Bode, M.F., Longmore, A.J., Admason, A.J., McFadzean, A.D., Aitken, D.K., & Roche, P.F. 1988, *MNRAS*, 233, 321
- Whittet, D.C.B., Gerakines, P.A., Hough, J.H., & Shenoy, S.S. 2001, *ApJ*, 547, 872
- Whittet, D.C.B., et al. 2007, *ApJ*, 655, 332
- Whittet, D.C.B., Hough, J.H., Lazarian, A., & Hoang, T. 2008, *ApJ*, in press

Table 1. Catalog of reddened field stars and associated data^a

2MASS	Other name ^b	Sp.	$J-H$	$H-K_s$	K_s	[3.6]	[4.5]	[5.8]	[8.0]	[12]	A_V
J04082673+2803429			1.17	0.50	9.60						6.4
J04090144+2453214			1.27	0.50	5.73						4.4
J04092063+2816031			1.27	0.43	7.45						4.1
J04104300+2820340			1.33	0.47	9.84						4.6
J04110488+2443185			1.15	0.44	8.12						3.5
J04112677+2831093			1.07	0.42	9.00						5.5
J04112801+2830271			1.17	0.45	9.94						3.7
J04113168+2829562	JH 126		0.90	0.40	8.74						4.5
J04114185+2841282	IRAS 04085+2833		1.11	0.47	5.09					4.60	5.9
J04114938+2815568			1.16	0.45	9.24						3.6
J04122296+2949441			1.09	0.43	9.99						5.6
J04123318+2945152			1.32	0.53	9.25						4.8
J04123940+2816419			1.64	0.62	8.85						7.0
J04130664+2235365			1.03	0.40	7.53						5.2
J04132688+2804584			1.11	0.52	9.54						6.3
J04132993+2943325			1.04	0.41	9.20						5.3
J04133166+2806130			2.25	1.11	9.19						15.2
J04134374+2821547		K3 III ^d	1.74	0.73	7.65						8.4
J04134868+2823436			1.28	0.51	6.66						4.5
J04135352+2813056			3.90	2.06	9.92						28.7
J04135912+2822182			1.32	0.50	9.60						4.7
J04140174+2808577			2.98	1.53	9.84						21.2
J04143434+2802406			1.29	0.59	8.97						7.5
J04144359+2817086			2.84	1.36	8.03					6.83 ^e	17.0
J04152407+2807074			0.88	0.44	9.18						6.3
J04152859+2451554	IRAS 04124+2444		1.03	0.43	4.74					4.49	5.3
J04152950+2818313			0.95	0.41	9.70						4.8
J04154949+2851175			1.39	0.60	9.82						5.5
J04162595+2808443			1.31	0.51	8.66						4.6
J04163376+2854051			0.91	0.41	8.80						4.6
J04163442+2802386	JH 167		1.08	0.42	7.20						3.0
J04163846+2853573			1.04	0.40	9.50						2.7
J04170129+2839143			1.96	0.97	9.65						12.9
J04170178+2821593			1.79	0.76	8.53	8.07	8.13	7.93	7.95		8.5
J04173477+2757338			1.37	0.63	9.78	9.55	9.40	9.31	9.29		8.2
J04173746+2811230			1.82	0.76	9.35	8.90	8.85	8.73	8.74		8.6
J04174322+2747396			1.14	0.48	9.78	9.49	9.49	9.40	9.39		6.2
J04180306+2840528			0.79	0.46	9.87						5.9
J04181078+2519574			1.16	0.56	9.03						6.6
J04183702+2434105			1.09	0.42	6.67						3.0
J04184535+2826400	V410 Anon 9	A2	1.49	0.81	7.91	7.33	7.26	7.14	7.14		11.8
J04184767+2834011			1.19	0.47	9.65						3.9
J04192736+2813012			1.55	0.58	8.16	7.83	7.96	7.72	7.71		6.3
J04195830+2812139			1.32	0.46	7.50	7.15	7.23	7.09	7.10		4.5
J04203249+2721322			1.03	0.41	8.49	8.24	8.40	8.23	8.21		5.3
J04203895+2706404			1.38	0.60	8.96						5.5

Table 1—Continued

2MASS	Other name ^b	Sp.	$J-H$	$H-K_s$	K_s	[3.6]	[4.5]	[5.8]	[8.0]	[12]	A_V
J04204138+2705474			1.28	0.55	7.68						7.3
J04205771+2516184			1.27	0.49	8.63						4.3
J04205996+3022179			0.96	0.40	6.22						4.8
J04211454+2703302			1.63	0.72	9.21						7.4
J04213256+2657270			1.69	0.78	9.24						8.1
J04214879+2832553			1.25	0.50	8.21	7.83	7.89	7.79	7.76		4.3
J04223539+2504186			1.16	0.43	9.43						3.5
J04231777+2806260			1.08	0.46	6.52	6.30	6.43	6.26	6.20		5.8
J04231783+2508529			0.95	0.46	9.63						6.7
J04232455+2500084	Elias 3	K2 III	1.74	0.78	5.81						9.2
J04234626+2642457	GJL 0420.7+2636	K5 III ^d	1.86	0.80	9.31	8.83	8.73	8.61	8.56		8.8
J04251866+2555359			1.04	0.44	6.82	6.52	6.55	6.31	6.19		5.4
J04253953+2544592	IRAS 04225+2538		1.04	0.41	5.21	—	—	4.99	4.94	5.06	5.3
J04254287+2635535			1.08	0.41	9.79	9.52	9.52	9.37	9.43		2.9
J04255543+2709122			1.12	0.46	8.01	7.74	7.73	7.62	7.65		5.9
J04261745+2436588			1.65	0.68	9.27	8.92	8.91	8.73	8.77		7.3
J04262182+2652111			1.25	0.41	8.46	8.19	8.28	8.17	8.13		3.8
J04263071+2436372			2.85	1.38	7.62	6.79	6.74	6.48	6.39	6.41 ^e	17.8
J04263650+2439469			2.27	1.11	9.59						15.3
J04274283+2622567			1.44	0.58	7.36	6.98	7.14	6.95	6.94		5.7
J04274738+2442267			1.16	0.45	9.98	9.67	9.61	9.53	9.54		3.6
J04274755+2624181			1.21	0.41	8.32	8.01	8.06	7.96	7.92		3.6
J04275374+2617222			1.13	0.43	9.62	9.32	9.29	9.19	9.19		3.3
J04275776+2440599			1.63	0.68	8.76	8.37	8.33	8.13	8.12		7.2
J04280463+2438411			1.34	0.56	9.11	8.82	8.77	8.67	8.61		5.1
J04280994+2432059			1.13	0.42	8.84	8.55	8.55	8.42	8.47		3.3
J04281255+2440431			1.25	0.55	9.01	8.79	8.71	8.62	8.59		7.1
J04282062+2653387			1.33	0.51	7.75	7.35	7.44	7.30	7.30		4.8
J04285007+2438275			1.30	0.52	9.12	8.80	8.75	8.64	8.65		4.7
J04285165+2433477			1.23	0.52	8.76	8.40	8.35	8.34	8.29		6.8
J04290729+2659136			1.27	0.48	9.18	8.85	8.86	8.76	—		4.3
J04291286+2442532			1.54	0.65	9.41						6.6
J04292083+2742074	IRAS 04262+2735	YSO? ^f	1.09	0.45	7.02	6.55	6.50	6.15	5.01	3.90	5.0
J04293024+2723521			1.29	0.46	7.32	6.92	7.22	7.01	7.01		4.3
J04293024+2658276			2.26	1.02	8.13	7.45	7.57	7.27	7.27	6.96 ^e	11.5
J04294376+2701532			1.37	0.51	8.74	8.40	8.43	8.30	8.32		5.0
J04294411+2438446			1.21	0.41	8.36	8.18	8.27	8.10	8.09		3.6
J04294651+2431493			1.81	0.77	9.55	9.12	8.92	8.80	8.81		8.6
J04295364+2332364			1.27	0.50	6.26	—	6.11	5.93	5.89		4.4
J04295531+2258579	IRAS 04269+2252		1.14	0.53	4.72	—	—	4.35	4.18	3.49	6.5
J04301480+2717460			1.15	0.41	8.59	8.37	8.43	8.33	8.32		3.3
J04302414+2819165			1.20	0.44	7.14	6.80	6.85	6.65	6.54		3.7
J04303410+2711046			1.25	0.44	8.21	7.89	8.01	7.87	7.82		4.0
J04303867+2255520			1.55	0.77	7.74	7.31	7.27	7.14	7.12		9.8
J04304246+2258248			1.21	0.53	8.14	7.76	7.83	7.70	7.67		6.8
J04304284+2743299			1.05	0.52	7.67	6.92	6.97	6.71	6.62		7.6

Table 1—Continued

2MASS	Other name ^b	Sp.	$J-H$	$H-K_s$	K_s	[3.6]	[4.5]	[5.8]	[8.0]	[12]	A_V
J04305298+2409541			1.23	0.48	9.83	9.52	9.46	9.41	9.39		4.1
J04305335+2709552			1.08	0.41	9.57	9.27	9.29	9.22	9.21		3.0
J04305639+2409078			1.21	0.51	8.40	8.12	8.14	8.02	8.00		6.7
J04312113+2658422	IRAS 04282+2652		1.23	0.63	4.91	—	—	4.36	4.19	3.86	7.4
J04312636+2707204	JH 57		0.92	0.45	8.23	8.05	7.93	7.84	7.85		6.5
J04313158+2439424			1.09	0.44	6.41	6.18	6.32	6.18	6.14		5.7
J04314179+2440149			1.33	0.48	8.93	8.65	8.78	8.58	8.57		4.7
J04314202+2704049			1.16	0.47	9.43	9.16	9.15	9.06	9.00		6.2
J04314783+2415023			1.53	0.59	9.62	9.20	9.28	9.09	9.10		6.2
J04314862+2706170			1.04	0.48	9.26	8.95	8.92	8.82	8.86		5.6
J04315067+2659412	JH 64		1.00	0.41	8.89	8.62	8.76	8.72	8.64		5.0
J04315117+2443449			1.32	0.45	7.99	7.68	7.80	7.67	7.62		4.4
J04315860+2412552			1.15	0.44	9.12	8.86	8.91	8.77	8.77		3.5
J04320127+2813347			1.15	0.40	6.89	6.63	6.82	6.64	6.63		3.3
J04320792+2432106			1.41	0.54	7.97	7.59	7.63	7.50	7.47		5.4
J04320816+2405482			1.18	0.43	9.79	9.49	9.54	9.43	9.40		3.6
J04321130+2613237			1.09	0.41	9.23	8.94	9.01	8.89	8.83		3.0
J04321153+2433380	Elias 9	M4 III	1.53	0.58	5.48	—	—	5.06	5.01	5.22 ^e	4.9
J04321327+2429107			3.46	1.78	8.12	7.06	6.77	6.54	6.52	6.60 ^e	22.5
J04321380+2630461			1.30	0.45	9.26	8.94	9.00	8.90	8.84		4.3
J04322815+2711228			1.44	0.60	7.16	6.70	6.77	6.53	6.40		5.8
J04323594+2253112			1.31	0.54	7.05						4.8
J04323842+2648098			1.21	0.42	8.88	8.62	8.67	8.60	8.57		3.7
J04323892+2358251	Elias 10	M8 III	1.17	0.54	5.81	—	—	4.83	4.65	4.49	2.2
J04323908+2700083	IRAS 04295+2653		1.03	0.41	4.89	—	—	4.69	4.64	4.74	5.2
J04324166+2419038			1.19	0.59	8.88	8.58	8.36	8.35	8.35		7.0
J04325815+2525324			1.11	0.43	8.00	7.81	7.95	7.78	7.73		3.2
J04330802+2556436			1.50	0.65	8.65	8.19	8.19	8.05	8.04		6.4
J04330971+2656220		K8 III ^d	1.41	0.54	6.85	6.49	6.61	6.45	6.41		5.0
J04332164+2239504	JH 114		1.10	0.42	7.19						3.1
J04332594+2615334	Elias 13	K2 III	2.03	0.97	5.56	—	—	4.78	4.76	4.90	11.7
J04332662+2410446			1.17	0.41	8.59	8.35	8.41	8.29	8.25		3.4
J04333234+2425120			1.22	0.45	8.13	7.72	7.82	7.75	7.70		3.9
J04333734+2247505			1.35	0.50	8.12						4.8
J04333776+2612591			1.06	0.57	9.33	8.95	8.83	8.76	8.78		7.9
J04334115+2408100			1.20	0.48	9.94	9.64	9.59	9.53	9.49		4.0
J04334465+2615005			1.25	0.64	9.74						9.3
J04335006+2408216			1.11	0.46	9.21	8.91	8.95	8.82	8.82		5.9
J04335113+2615115			1.17	0.48	8.43	8.05	8.03	7.99	7.94		3.8
J04335142+2718339			1.18	0.44	8.63	8.28	8.51	8.36	8.31		3.6
J04340563+2734335			1.24	0.49	6.09	—	6.00	5.80	5.78		4.2
J04341640+2651195			1.34	0.51	9.21	8.89	8.95	8.85	8.85		4.8
J04342761+2706433			1.32	0.49	9.86	9.50	9.54	9.43	9.40		4.6
J04343077+2541497			1.26	0.43	7.75	7.45	7.60	7.45	7.44		4.0
J04343120+2653363			0.73	0.42	9.79	9.49	9.46	9.41	9.44		5.4
J04343230+2250218			1.11	0.42	9.05						3.1

Table 1—Continued

2MASS	Other name ^b	Sp.	$J-H$	$H-K_s$	K_s	[3.6]	[4.5]	[5.8]	[8.0]	[12]	A_V
J04343549+2644062			1.30	0.52	6.89	6.49	6.58	6.43	6.20		4.7
J04343848+2242133			1.05	0.44	6.89						5.5
J04344389+2655155			1.25	0.49	9.55	9.21	9.20	9.08	9.07		4.2
J04344754+2657083			1.42	0.49	9.03	8.73	8.75	8.63	8.61		5.1
J04351798+2402459			1.15	0.53	9.15	8.84	8.85	8.75	8.73		6.5
J04352020+2232146			0.96	0.51	9.73						7.1
J04352271+2647297			1.21	0.43	9.54	9.21	9.27	9.16	9.15		3.7
J04352370+2404502			2.40	1.25	8.51	7.75	7.65	7.43	7.42		16.7
J04352820+2250257			1.09	0.41	8.13						3.0
J04353751+2405332			2.00	0.95	9.37	8.81	8.78	8.58	8.57		10.6
J04353776+2403348			1.61	0.67	9.29	8.93	8.91	8.77	8.78		7.1
J04354848+2251341			1.29	0.46	9.43						4.3
J04355684+2254360			1.09	0.52	9.53						6.1
J04361252+2413387			1.13	0.42	9.79	9.56	9.64	9.53	9.52		3.3
J04363003+2318383			1.17	0.48	6.79	6.48	6.72	6.52	6.49		6.3
J04363513+2526425			1.08	0.43	7.12	6.83	6.92	6.80	6.78		5.6
J04364224+2555117	IRAS 04336+2549		1.17	0.40	5.26	—	—	4.74	4.65	4.72	3.4
J04365561+2336594			1.23	0.51	6.80	6.20	6.36	6.33	5.98		4.3
J04365910+2619418			1.48	0.52	6.76	6.38	6.52	6.36	6.34		5.6
J04371368+2422208			1.11	0.42	6.86	6.50	6.73	6.58	6.57		3.2
J04371558+2616155			1.29	0.45	8.11	7.75	7.84	7.72	7.69		4.3
J04371580+2629295			1.89	0.88	9.94	9.52	9.34	9.18	9.15		9.6
J04371735+2255406			1.02	0.41	8.74						5.2
J04372471+2627285			1.88	0.79	7.62	7.10	7.20	6.99	6.98		9.1
J04372821+2610289	TNS 2; Kim 6	M0 III ^c	1.63	0.67	6.70	6.29	6.40	6.19	6.17	6.04 ^e	6.6
J04372946+2609509			1.08	0.43	9.91	9.62	9.58	9.51	9.50		5.6
J04373457+2625518			1.15	0.41	8.37	8.14	8.24	8.06	8.01		3.3
J04375136+2623585			1.09	0.41	7.13	6.88	6.96	6.82	6.81		3.0
J04375850+2602497			1.32	0.49	9.65	9.44	9.35	9.28	9.27		4.6
J04375986+2528090	IRAS 04349+2522	M3 III ^c	1.21	0.50	5.20	—	—	4.90	4.89	4.78	2.9
J04383741+2547138			1.10	0.42	9.66	9.36	9.41	9.31	9.29		3.1
J04383928+2551062	Kim 23	K1 III ^c	1.35	0.57	9.13	8.71	8.73	8.65	8.65		6.4
J04383931+2608508			1.30	0.55	9.96	9.64	9.67	9.55	9.50		4.8
J04383974+2619310			1.17	0.41	9.57	9.27	9.34	9.24	9.20		3.4
J04384018+2639382			1.55	0.66	7.30	6.88	6.92	6.73	6.72		6.7
J04384470+2518004			1.27	0.43	8.12	7.87	7.94	7.77	7.74		4.1
J04385148+2534172	TNS 10; Kim 30	M0 III ^c	1.21	0.45	4.87	—	—	4.59	4.59	4.58	3.3
J04385153+2559441	Kim 29	K3 III ^c	1.29	0.50	7.38	7.04	7.10	6.98	6.98		5.0
J04385827+2631084	Elias 14	M5 III	1.72	0.80	6.89	6.35	6.37	6.15	5.98		6.7
J04390593+2550079	Kim 32	K0 III ^c	1.73	0.75	8.17	7.68	7.64	7.48	7.49		8.1
J04390696+2627199	JH 214		0.95	0.48	9.09	8.73	8.64	8.60	8.65		9.6
J04390745+2553544			3.10	1.50	9.97	9.00	8.85	8.61	8.58		19.1
J04390885+2614103			1.38	0.59	9.84	9.50	9.46	9.39	9.33		5.5
J04391820+2544326			1.58	0.63	9.53	9.06	9.11	8.97	8.98		6.7
J04392692+2552592	Elias 15	M2 III	2.75	1.28	6.91	6.08	6.10	5.81	5.79	5.93 ^e	15.3
J04392986+2618317			1.13	0.49	9.97	9.64	9.61	9.55	9.50		6.2

Table 1—Continued

2MASS	Other name ^b	Sp.	$J-H$	$H-K_s$	K_s	[3.6]	[4.5]	[5.8]	[8.0]	[12]	A_V
J04393558+2628396			1.01	0.44	9.82	9.52	9.45	9.38	9.43		5.3
J04393779+2613567			1.49	0.64	9.68	9.28	9.27	8.99	9.10		6.3
J04393890+2611250	Elias 16	K1 III	3.64	1.81	5.16	—	—	3.56	3.54	3.72	24.1
J04394383+2535450			1.70	0.66	9.98	9.59	9.52	9.39	9.38		7.5
J04394395+2516013	Elias 17	M5 III	1.44	0.62	6.56	6.18	6.40	6.14	6.15		4.3
J04400300+2528176			1.50	0.64	9.42	8.98	9.00	8.85	8.83		6.4
J04401230+2613203	JH 216; Kim 45	G8 III ^c	1.07	0.43	8.30	7.98	8.01	7.89	7.92		4.7
J04401383+2559163	Kim 46	K5 III ^c	1.79	0.71	7.44	7.01	7.03	6.84	6.85		8.0
J04403830+2554274	GKH 7		1.05	0.42	9.06						5.3
J04404541+2531566	Kim 49	G4 III ^c	1.94	0.84	9.33						11.6
J04405597+2531312	Kim 52	K2 III ^c	1.61	0.70	7.22						8.1
J04405690+2601043			1.76	0.72	8.76	8.34	8.43	8.17	8.14		8.1
J04405745+2554134	TNS 8	K5 III	3.37	1.71	7.46	6.38	6.17	5.94	5.87		21.5
J04405845+2612306			1.20	0.48	9.80	9.45	9.50	9.44	9.37		3.9
J04410274+2539470	TNS 12		1.33	0.58	5.20	—	—	4.83	4.80	4.95	6.9
J04410544+2541078			1.12	0.42	9.66	9.33	9.37	9.27	9.25		3.2
J04411845+2401576			1.12	0.43	6.58	6.28	6.28	6.11	5.94		3.2
J04412285+2556199			1.03	0.48	9.58	9.28	9.16	9.11	9.08		5.6
J04413015+2527019	Kim 59	K2 III ^c	2.01	0.89	7.63	6.99	7.02	6.85	6.83		11.2
J04413108+2519222			1.85	0.79	9.50	8.97	8.97	8.77	8.73		8.9
J04413486+2500544			1.54	0.65	9.24	8.79	8.74	8.60	8.57		6.6
J04413630+2502062			1.29	0.51	8.94	8.55	8.57	8.48	8.45		4.6
J04413973+2505583			1.25	0.41	8.36	8.06	8.19	8.02	7.98		3.8
J04415119+2602090			1.10	0.40	9.43	9.20	9.31	9.20	9.16		3.0
J04415321+2449158			1.16	0.44	7.82	7.58	7.67	7.47	7.41		3.5
J04415533+2515092			1.04	0.41	9.67	9.43	9.35	9.30	9.25		5.3
J04415802+2600435			1.17	0.42	7.56	7.26	7.45	7.26	7.28		3.5
J04420337+2540258	JH 218		0.92	0.42	8.90	8.59	8.56	8.52	8.54		4.7
J04420618+2543246			1.10	0.41	9.79	9.57	9.54	9.44	9.43		3.1
J04421818+2536207			1.43	0.60	9.83	9.42	9.42	9.30	9.25		5.8
J04421841+2516532	Kim 65	K1 III ^c	1.06	0.44	8.68	8.38	8.39	8.29	8.25		4.3
J04422934+2517425	GKH 21		1.25	0.52	8.86	8.54	8.60	8.46	8.46		4.4
J04423570+2527152	IRAS 04395+2521	K5 III ^c	1.27	0.52	5.50	—	—	5.10	5.13	5.12	4.4
J04424107+2505064			1.37	0.52	9.61	9.22	9.34	9.23	9.21		5.0
J04425915+2507206			1.10	0.42	9.11	8.80	8.79	8.72	8.68		3.1
J04430048+2459230	IRAS 04399+2453		1.12	0.41	5.48	—	—	5.18	5.19	5.15	3.2
J04430889+2504490			1.13	0.43	9.62	9.31	9.42	9.28	9.27		3.3
J04431258+2521027	GKH 25		1.22	0.43	9.00	8.76	8.76	8.64	8.65		3.8
J04431538+2444558			1.27	0.54	6.80	6.49	6.65	6.46	6.39		4.6
J04434337+2523257	GKH 27; Kim 84		1.11	0.41	7.33	7.04	7.15	7.02	7.02		3.1
J04434870+2457306			1.15	0.46	6.14	—	6.06	5.90	5.84		3.6
J04441137+2459355			1.22	0.43	8.43	8.13	8.31	8.14	8.10		3.8
J04441794+2524512	Elias 19	M4 III	1.18	0.46	6.05	—	5.94	5.71	5.65		2.5
J04443504+2501082	IRAS 04415+2455		1.28	0.52	5.97	—	5.66	5.42	5.29	5.25	4.6
J04445592+2509204			1.15	0.40	7.92	7.73	7.79	7.66	7.64		3.3
J04450980+2503186			1.31	0.45	7.76	7.47	7.59	7.42	7.43		4.3

Table 1—Continued

2MASS	Other name ^b	Sp.	$J-H$	$H-K_s$	K_s	[3.6]	[4.5]	[5.8]	[8.0]	[12]	A_V
J04451569+2449525			1.22	0.41	6.58	6.31	6.42	6.29	6.26		3.7
J04451757+2446027			1.16	0.42	6.01	—	5.92	5.76	5.70		3.4
J04452612+2501590			1.13	0.44	9.77	9.48	9.49	9.42	9.37		3.4
J04453986+2517045			1.18	0.45	8.46	8.19	8.25	8.05	7.94		3.7
J04461799+2507138			1.16	0.41	7.77	7.49	7.65	7.50	7.46		3.4
J04463986+2425260	IRAS 04435+2419		1.13	0.40	5.87	—	5.55	5.35	5.22	4.98	3.2
J04471909+2448510			1.23	0.41	7.08	6.85	6.97	6.81	6.79		3.7
J04472659+2605172			1.07	0.40	5.63	—	5.65	5.42	5.42		2.9
J04475068+2529299			1.19	0.41	9.56	9.26	9.30	9.22	9.19		3.5
J04475454+2523191			1.24	0.42	9.65	9.37	9.48	9.35	9.31		3.8
J04475943+2537551			1.04	0.44	9.83	9.62	9.53	9.34	9.46		5.4
J04480327+2540079			1.09	0.44	9.69	9.40	9.38	9.34	9.30		5.7
J04480380+2521488	GKH 30		1.27	0.46	7.89	7.53	7.75	7.55	7.54		4.2
J04481020+2537537			1.17	0.45	8.95	8.60	8.54	8.57	8.51		3.6
J04481911+2545075	GKH 15		1.15	0.42	7.03	6.73	6.90	6.71	6.73		3.4
J04482478+2524559			1.41	0.51	7.83	7.46	7.59	7.40	7.35		5.2
J04484817+2538123	Elias 21	M2III	1.21	0.46	6.21	—	6.11	5.95	5.88		3.1
J04494966+2538435			1.14	0.41	7.32	7.12	7.27	7.08	7.06		3.3
J04512418+2520029	IRAS 04483+2514		1.12	0.50	5.53					4.72	6.1

^aSpectral classifications (col. 3) are from SIMBAD unless otherwise noted. Photometry in the JHK_s passbands (cols. 4–6) is from the 2MASS catalog; photometry in the 3.6–8.0 μm passbands (cols. 7–10) is from Spitzer IRAC observations; photometry at 12 μm (col. 11) is calculated from flux data in the IRAS Point Source Catalog (version 2.0) unless otherwise noted; dashes in the photometry columns indicate saturation, empty fields indicate no data available. Visual extinction estimates from the current work are listed in the final column.

^bKey to identifications: Elias – Elias 1978; GJL – Goodman et al. 1992; GKH – Gomez, Kenyon, & Hartmann 1994; IRAS – Infrared Astronomical Satellite Point Source Catalog; JH – Jones & Herbig 1979; Kim – unpublished catalog cited by Murakawa et al. 2000; TNS – Tamura et al. 1987; V410 Anon 9 – Strom & Strom 1994.

^cSpectral classification from Murakawa et al. 2000.

^dSpectral classification from Shenoy 2003.

^ePhotometry simulated from Spitzer IRS 9.9–19.6 μm calibrated flux spectra (Whittet et al. 2007).

^fExcess infrared flux at $\lambda > 5 \mu\text{m}$ suggests this star to be a YSO (see §5).

Table 2. YSOs with high estimated extinction^a

2MASS	Other name	Sp ^b	A_V
J04182239+2824375	V410 Anon 24		18.9
J04182909+2826191	V410 Anon 25		21.8
J04183444+2830302	V410 X-ray 2		19.6
J04184023+2824245	V410 X-ray 4		16.4
J04184133+2827250	LR1		22.8
J04184505+2820528	V410 Anon 20		19.1
J04323205+2257266	IRAS 04295+2251		18.5
J04395574+2545020	Elias 18; IC 2087 IR	B5	22.2
J04400800+2605253	IRAS 04370+2559		12.5
J04412464+2543530	ITG 40	M3.5	21.7

^aBased on photometry listed in Luhman et al. 2006.

^bSpectral types are from SIMBAD (Elias 18) and Luhman et al. 2006 (ITG 40); intrinsic colors appropriate to an M0 dwarf are assumed in all other cases.

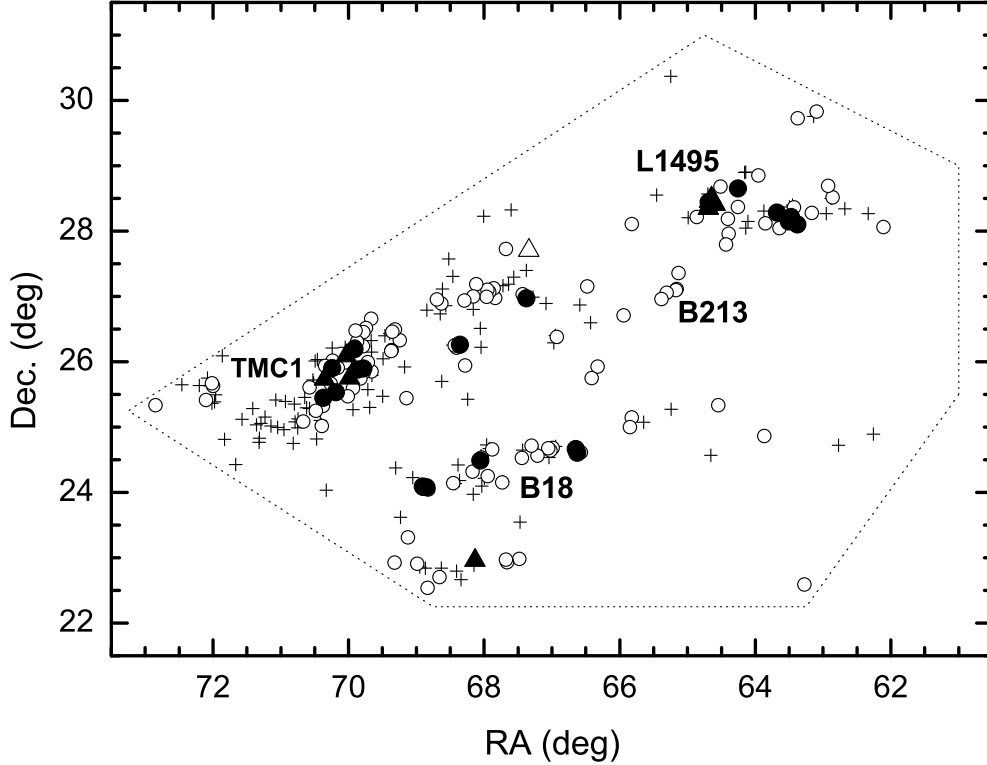


Fig. 1.— Map of the distribution of field stars identified in this work (Table 1; J2000 coordinates). Dotted lines denote the boundaries of the survey area. Symbols used for field stars are coded by visual extinction: plus signs ($2 < A_V < 5$); open circles ($5 < A_V < 10$); filled circles ($A_V > 10$). The YSO candidate J04292083+2742074 is denoted by an open triangle. Ten highly reddened YSOs listed in Table 2 are also plotted (filled triangles; six of them are clustered together in L 1495). The vertices of the hexagonal survey area are located at RA, Dec. (2000, counterclockwise from the left): 04h 53m, +25° 15'; 04h 35m, +22° 15'; 04h 13m, +22° 15'; 04h 04m, +25° 30'; 04h 04m, +29° 00'; and 04h 19m, +31° 00'.

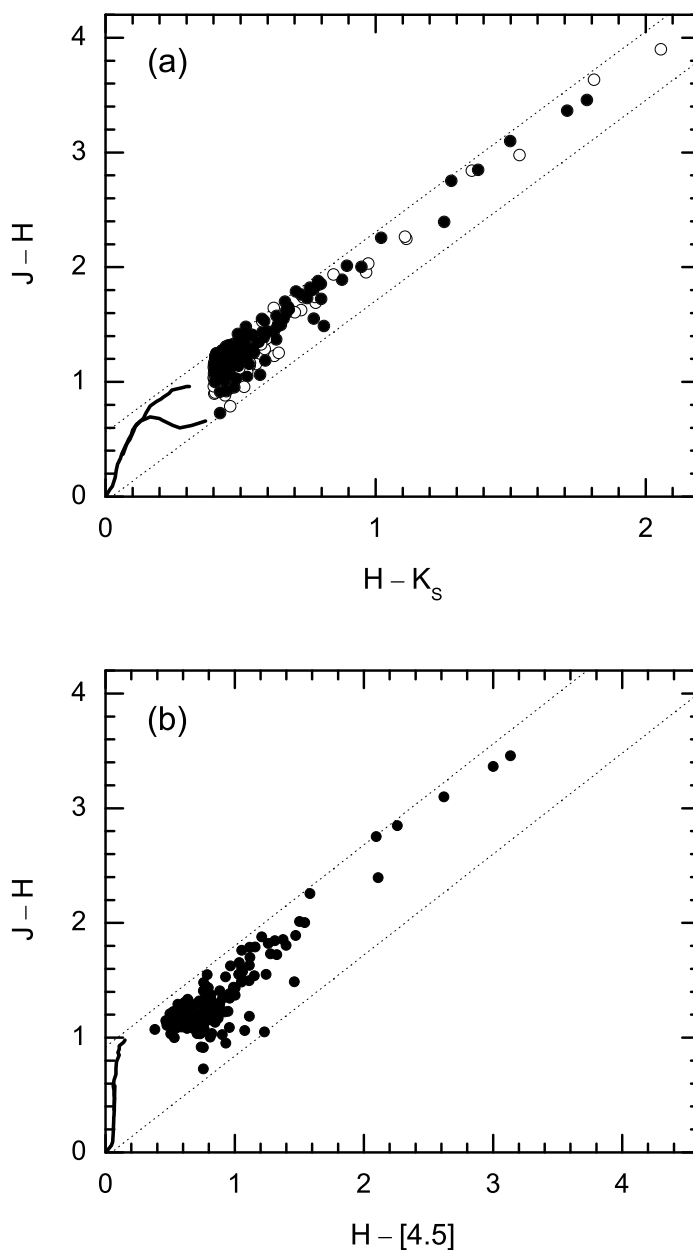


Fig. 2.— Color-color diagrams for candidate reddened field stars listed in Table 1: (a) $J-H$ vs. $H-K_s$, and (b) $J-H$ vs. $H-[4.5]$. Open circles in frame (a) denote stars that lack $4.5\ \mu\text{m}$ photometry and therefore do not appear in frame (b). Solid curves near the origin represent intrinsic colors for normal stars. The dotted diagonal lines in each frame are parallel to the appropriate reddening vector and indicate the approximate upper and lower boundaries of the zone occupied by normal reddened stars lacking circumstellar infrared emission.

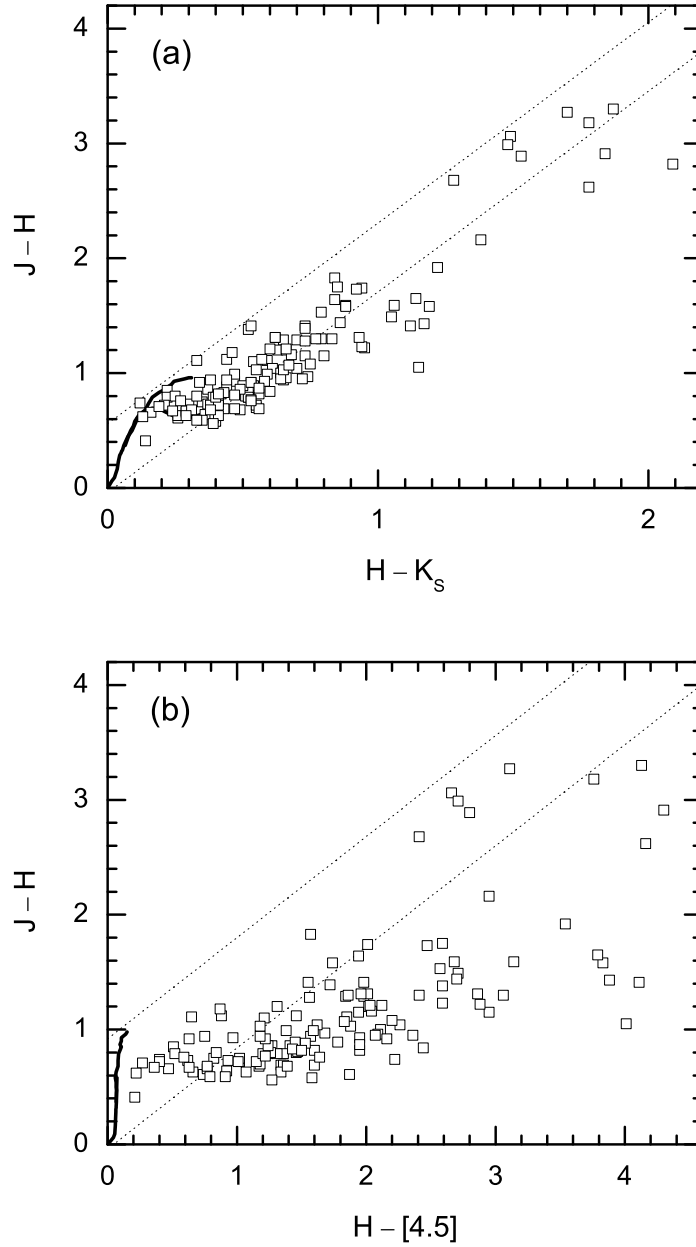


Fig. 3.— Color-color diagrams exactly analogous to those in Fig. 2, but here plotted for known members of the Taurus star-forming region. The data are from Tables 2 and 4 of Luhman et al. (2006); only stars with photometry available in all four relevant passbands are included.

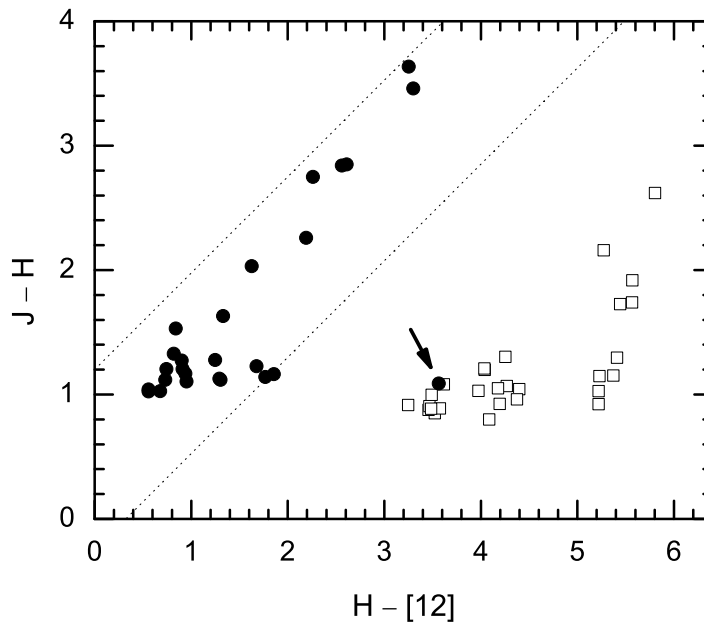


Fig. 4.— The $J - H$ vs. $H - [12]$ color-color diagram. Filled circles and open squares denote candidate field stars (Table 1) and previously known YSOs (Luhman et al. 2006), respectively. All $12\mu\text{m}$ data for YSOs are taken from the IRAS Point Source Catalog. As before, the dotted diagonal lines indicate the approximate upper and lower boundaries of the expected distribution for normal reddened stars. The datum for the anomalous object IRAS 04262+2735 (J04292083+2742074) is arrowed.

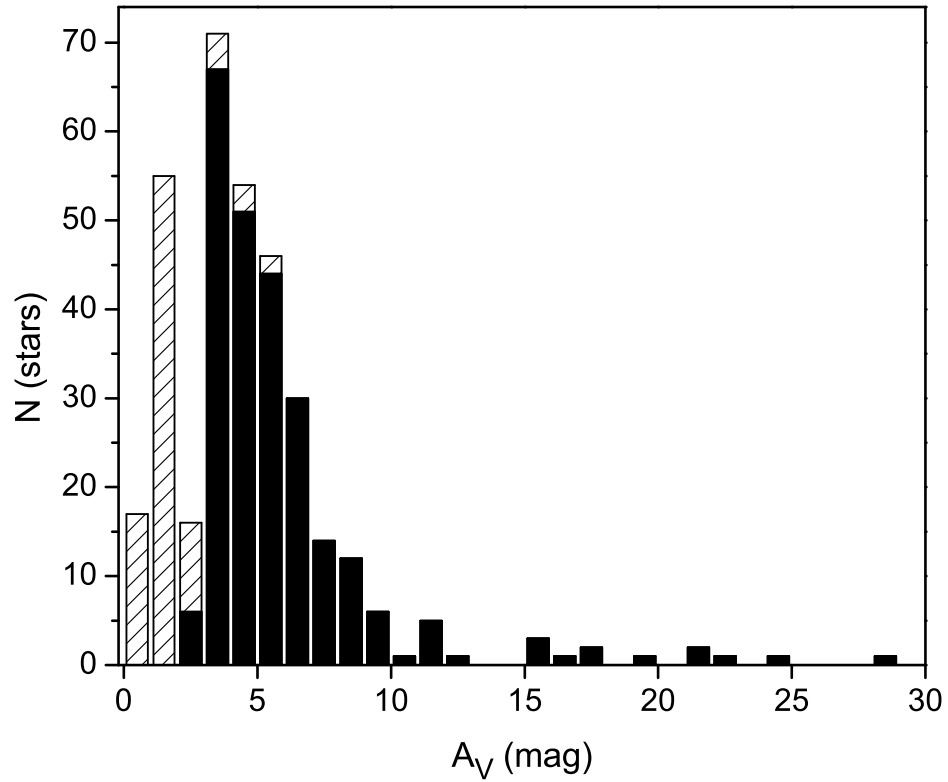


Fig. 5.— Histogram of 249 extinction values from Table 1 divided into 1-magnitude bins (black columns). Also shown (shaded) is the effect of adding extinction data for 81 optically-selected reddened stars from the literature (Straizys & Meistas 1980; Whittet et al. 2001) to our data. The total height of each column in the region of overlap (2–6 mag) sums the contributions of optical and infrared samples.

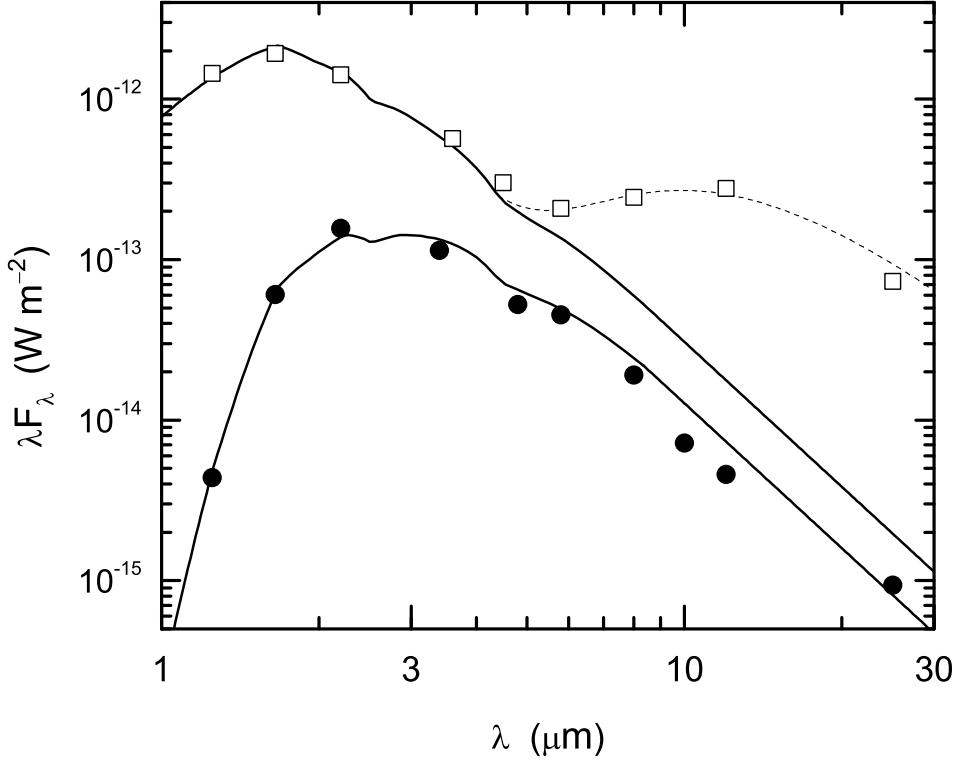


Fig. 6.— Spectral energy distribution for the new YSO candidate IRAS 04262+2735 (J04292083+2742074, open squares) compared with that of the highly reddened field star Elias 16 (J04393890+2611250, solid circles), combining 2MASS, IRAC and IRAS photometry. Additional ground-based 3.4–10 μm photometry from Elias (1978) is included for the latter object as three of the four IRAC bands are saturated. Photometric errors are comparable with the size of the plotting symbols. A color correction appropriate to a 4500 K blackbody has been applied to the IRAS data for each source. Flux data for Elias 16 have been divided by a factor of 50 for display. Models (curves) were constructed assuming each star to have an intrinsic spectrum with $T_{\text{eff}} = 4500$ K (Kurucz 1992) subject to extinction $A_V = 5$ mag (IRAS 04262+2735) and $A_V = 24$ mag (Elias 16). The dashed curve shows the effect of adding thermal emission from warm dust ($T_{\text{dust}} = 350$ K) to the model for IRAS 04262+2735, scaled to match the observed mid-infrared flux.